6-13-2018

The Origin of the Prompt Emission for Short GRB 170817A: Photosphere Emission or Synchrotron Emission?

Yan-Zhi Meng
Chinese Academy of Sciences

Jin-Jun Geng
Nanjing University, gengjinjun@nju.edu.cn

Bin-Bin Zhang
Nanjing University, zhang.grb@gmail.com

Jun-Jie Wei
Chinese Academy of Sciences

Di Xiao
Nanjing University

The Astrophysical Journal, 860:72 (11pp), 2018 June 10 https://doi.org/10.3847/1538-4357/aac2d9

The Origin of the Prompt Emission for Short GRB 170817A: Photosphere Emission or Synchrotron Emission?

Yan-Zhi Meng[1,2], Jin-Jun Geng[3,4], Bin-Bin Zhang[3,4], Jun-Jie Wei[1], Di Xiao[3,4], Liang-Duan Liu[3,4], He Gao[5], Xue-Feng Wu[1], En-Wei Liang[6], Yong-Feng Huang[3,4], Zi-Gao Dai[3,4], and Bing Zhang[7]
[1] Purple Mountain Observatory, Chinese Academy of Sciences, Nanjing 210008, People's Republic of China; xfwu@pmo.ac.cn
[2] University of Chinese Academy of Sciences, Beijing 100049, People's Republic of China
[3] School of Astronomy and Space Science, Nanjing University, Nanjing 210093, People's Republic of China; gengjinjun@nju.edu.cn, zhang.grb@gmail.com
[4] Key Laboratory of Modern Astronomy and Astrophysics (Nanjing University), Ministry of Education, People's Republic of China
[5] Department of Astronomy, Beijing Normal University, Beijing 100875, People's Republic of China
[6] Department of Physics and GXU-NAOC Center for Astrophysics and Space Sciences, Guangxi University, Nanning 530004, People's Republic of China
[7] Department of Physics and Astronomy, University of Nevada, Las Vegas, NV 89154, USA
Received 2018 January 2; revised 2018 April 19; accepted 2018 May 3; published 2018 June 13

Abstract

The first gravitational-wave event from the merger of a binary neutron star system (GW170817) was detected recently. The associated short gamma-ray burst (GRB 170817A) has a low isotropic luminosity ($\sim 10^{47}$ erg s^{-1}) and a peak energy $E_p \sim 145$ keV during the initial main emission between -0.3 and 0.4 s. The origin of this short GRB is still under debate, but a plausible interpretation is that it is due to the off-axis emission from a structured jet. We consider two possibilities. First, since the best-fit spectral model for the main pulse of GRB 170817A is a cutoff power law with a hard low-energy photon index ($\alpha = -0.62^{+0.49}_{-0.54}$), we consider an off-axis photosphere model. We develop a theory of photosphere emission in a structured jet and find that such a model can reproduce a low-energy photon index that is softer than a blackbody through enhancing high-latitude emission. The model can naturally account for the observed spectrum. The best-fit Lorentz factor along the line of sight is $\sim$20, which demands that there is a significant delay between the merger and jet launching. Alternatively, we consider that the emission is produced via synchrotron radiation in an optically thin region in an expanding jet with decreasing magnetic fields. This model does not require a delay of jet launching but demands a larger bulk Lorentz factor along the line of sight. We perform Markov Chain Monte Carlo fitting to the data within the framework of both models and obtain good fitting results in both cases.

Key words: gamma-ray burst: general – gravitational waves – radiation mechanisms: thermal

1. Introduction

Recently, the first joint detection of a gravitational-wave (GW) event (GW170817; Abbott et al. 2017a) and short gamma-ray burst (GRB 170817A; Abbott et al. 2017b; Connaughton et al. 2017; Goldstein et al. 2017b; Savchenko et al. 2017) confirmed the hypothesis that mergers of double neutron stars (NS–NS) are the progenitor systems of short gamma-ray bursts (SGRBs; Eichler et al. 1989; Narayan et al. 1992; Mochkovitch et al. 1993; Nakar 2007; Berger 2014). Follow-up electromagnetic observations revealed a host galaxy of GRB 170817A at a distance of $\sim$40 Mpc (Coulter et al. 2017), as well as broadband emission (Abbott et al. 2017c). The isotropic-equivalent energy of GRB 170817A is $\sim 5 \times 10^{46}$ erg (Goldstein et al. 2017a; Zhang et al. 2018b), which is much smaller than that of a typical SGRB (10^{50} erg).

Previous observations of short GRB jet breaks suggested that the half-opening angle of a SGRB jet is $\leqslant 20^{\circ}$ (e.g., Fong et al. 2015). On the other hand, the GW signals are essentially isotropic, so the detection rate of a GW event associated with an on-axis burst should be quite low for binary NS mergers. However, the simultaneous detection of GRB 170817A and GW170817 indicates that the rate for such similar events is actually high (Zhang et al. 2018b). Such a high rate implies that the jet may be structured, with an angle-dependent luminosity and bulk Lorentz factor outside an uniform core, rather than a simple "top-hat" form with a sharp edge (Granot et al. 2017b). Emission from such a structured jet could thus be seen by an off-axis observer with a large viewing angle (e.g., Jin et al. 2017; Lamb & Kobayashi 2017; Lazzati et al. 2017a; Xiao et al. 2017; Kathirgamaraju et al. 2018). The low isotropic luminosity ($\sim 10^{47}$ erg s^{-1}) of the prompt emission for GRB 170817A (Goldstein et al. 2017a; Zhang et al. 2018b) supports this suggestion. A structured jet has also been favored by other recent theoretical (e.g., Sapountzis & Vlahakis 2014) and numerical (e.g., Aloy et al. 2005; Tchekhovskoy et al. 2008; Komissarov et al. 2010; Murguia-Berthier et al. 2017) studies within the NS–NS merger context. As the jet breaks out of the neutron-rich "dynamical ejecta" ejected during the merger (e.g., Hotokezaka et al. 2013; Rosswog 2013), some "lateral structure" could be developed that has a lower luminosity than the on-axis relativistic jet.

The prompt emission for GRB 170817A is shown to have two temporal components: a main pulse and a weak tail. The main pulse (-0.26 to 0.57 s) spectrum is well fitted by the cutoff power-law model with a low-energy photon index $\alpha = -0.61^{+0.34}_{-0.60}$, while the weak tail (0.95–1.79 s), with $\sim 1/3$ of the fluence of the main pulse, is well fitted by a blackbody model (Zhang et al. 2018b, see also Goldstein et al. 2017b).

The physical origin of the prompt emission of GRB 170817A is unknown. The exponential cutoff on the high-energy end, and the relatively hard low-energy photon index (i.e., $\alpha = -0.61$ for the time interval between -0.26 and 0.57 s) for the main pulse and the dominated blackbody in the weak tail, may support a possible photospheric origin of the emission (e.g., Goodman 1986; Paczynski 1986; Abramowicz et al. 1991; Thompson 1994;

Mészáros & Rees 2000; Mészáros 2002; Ryde 2004, 2005; Rees & Mészáros 2005; Abdo et al. 2009; Pe'er & Ryde 2011; Lundman et al. 2013; Deng & Zhang 2014; Bégué & Pe'er 2015; Gao & Zhang 2015; Pe'er et al. 2015) . On the other hand, the α index is also consistent with the typical $\alpha = -2/3$ segment of synchrotron radiation (Rybicki & Lightman 1979). It is therefore interesting to perform detailed modeling of the prompt emission using both photospheric and synchrotron models, especially within the framework of an off-axis structured jet.

This paper is organized as follows. In Section 2, we develop a model of off-axis photosphere emission from a structured jet. Then, we apply this model to perform a Markov Chain Monte Carlo (MCMC) fitting to the spectrum of the main pulse of GRB 170817A in Section 3. In Section 4, we apply the MCMC technique to fit the same spectrum using the synchrotron model. Section 5 presents some discussions and the conclusions are drawn in Section 6.

2. Off-axis Photosphere Model in a Structured Jet

In this section, we present the calculation of the time-integrated photospheric emission spectrum from a structured jet observed by an off-axis observer.

2.1. Jet Structure

The jet adopted here is a structured jet with an angle-dependent luminosity (the injected power at the base of the flow) and baryon loading parameter[8] outside a uniform core (e.g., Dai & Gou 2001; Rossi et al. 2002; Zhang & Mészáros 2002a; Kumar & Granot 2003), i.e.,

$$L(\theta) = \frac{L_0}{[(\theta/\theta_{c,L})^{2q} + 1]^{1/2}},$$
$$\eta(\theta) = \frac{\eta_0}{[(\theta/\theta_{c,\Gamma})^{2p} + 1]^{1/2}} + 1.2, \quad (1)$$

where θ is the angle measured from the jet axis, $\theta_{c,L}$ and $\theta_{c,\Gamma}$ are the half-opening angles for the luminosity core and the bulk Lorentz factor core ($\theta_{c,L} = \theta_{c,\Gamma}$ is considered in our calculation), L_0 and η_0 are corresponding constant values in the core, respectively, and q and p describe how the luminosity and the bulk Lorentz factor decreases outside the core. Figure 1 presents the shape of the luminosity and Lorentz factor structures and the best-fit parameters presented in Section 3.

2.2. Photosphere Emission Spectrum

In the traditional photosphere model, the photospheric radius $R_{\rm ph}$ is the radius where the scattering optical depth for a photon moving toward the observer is equal to unity ($\tau = 1$). However, one should realize that wherever there is an electron, a photon has a probability of being scattered there. For an expanding shell, photons can be last-scattered at any position in the shell with a probability depending on the position. This changes the traditional spherical shell photosphere to a probability photosphere discussed by several authors (Pe'er 2008; Beloborodov 2011; Pe'er & Ryde 2011; Lundman et al. 2013; Deng & Zhang 2014). Following the literature, we define a probability function $P_1(r, \Omega)$ as the probability for a photon being last-scattered at radius r and angular coordinate Ω. This

[8] Note that the baryon loading parameter η at the base of the flow is also the bulk Lorentz factor Γ in the saturated acceleration regime.

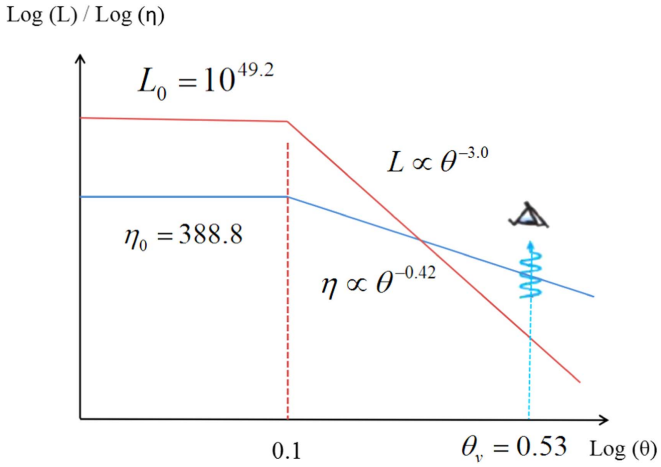

Figure 1. Jet structure and viewing angle for our photosphere model fitting of the main pulse spectrum (−0.3 to 0.4 s) of GRB 170817A. For our photosphere model fitting in Section 3, the best-fit values are $L_0 \sim 10^{49.16}$ erg s^{-1}, $\theta_{c,L} \sim 0.11$ rad, and $q \sim 2.99$ for the angular profile of luminosity; and $\eta_0 \sim 388.82$, $\theta_{c,\Gamma} \sim 0.11$ rad, and $p \sim 0.42^{+0.52}_{-0.07}$ for the angular profile of the bulk Lorentz factor, with a viewing angle $\theta_{\rm v} = 0.53$ rad. Thus, we get $L \sim 10^{47}$ erg s^{-1} and $\Gamma \sim 20$ at the line of sight. For the model calculation in Section 2.3, we take $L_0 = 10^{50}$ erg s^{-1}, $\theta_{c,L} = 0.1$ rad and $q = 3$ for the angular profile of luminosity, and $\eta_0 = 200$, $\theta_{c,\Gamma} = 0.1$ rad and $p = q/4 = 0.75$ for the angular profile of the bulk Lorentz factor. The viewing angle $\theta_{\rm v}$ is taken to be 0.8 rad to get $L \sim 10^{47}$ erg s^{-1} and $\Gamma \sim 26$ ($\eta \sim 40$) at the line of sight.

probability function may be calculated by (see Lundman et al. 2013)

$$P_1(r, \Omega) = (1 + \beta)D^2 \times \frac{R_{\rm ph}}{r^2} \exp\left(-\frac{R_{\rm ph}}{r}\right), \quad (2)$$

where β is the jet velocity and $D = [\Gamma(1 - \beta \cdot \cos\theta)]^{-1}$ is the Doppler factor.

In order to obtain the observed spectrum we need to know the probability of the observer-frame photon energy E when the photon undergoes the last scattering at (r, Ω). This photon energy distribution in the observer frame is determined by that in the comoving frame and $E = D(\Omega) \cdot E'$, where E' is the comoving frame photon energy. The photon energy distribution in the local comoving frame is assumed to be a Planck function with the same temperature as the electron due to the coupling of photons and electrons. Then, the photon temperature in the observer frame $T^{\rm ob}$ at (r, Ω) can be deduced from the plasma temperature $T'(r, \Omega)$ through $T^{\rm ob} = D(\Omega) \cdot T'(r, \Omega)$. Thus, we can get the distribution function $P_2(r, \Omega, E)$ of a photon of energy E and temperature $T^{\rm ob}$ at (r, Ω), which is described as

$$P_2(r, \Omega, E) = \frac{1}{2.40(kT^{\rm ob}(r, \Omega))^3} \frac{E^2}{\exp(E/kT^{\rm ob}(r, \Omega)) - 1}. \quad (3)$$

When calculating the observed time-integrated spectrum in the following, we adopt the spherical coordinates $(r, \Omega(\theta_{\rm LOS}, \phi_{\rm LOS}))$ corresponding to the line of sight (LOS). The observed time-integrated spectrum is a collection of the photons last-scattered at any position $(r, \theta_{\rm LOS}, \phi_{\rm LOS})$ and toward the observer, thus we must know the probability that the last-scattering occurred at $(r, \theta_{\rm LOS}, \phi_{\rm LOS})$, as well as the temperature at that location. This probability and temperature are determined by the luminosity and Lorentz factor in the direction $(\theta_{\rm LOS}, \phi_{\rm LOS})$, which depend completely on the angle θ of this direction to the jet axis. If the

angle between the jet axis and the LOS (i.e., the viewing angle) is θ_v, the corresponding angle θ follows

$$\theta = \theta(\theta_{\rm LOS}, \phi_{\rm LOS}) = \arccos[\cos(\theta_{\rm LOS})\cos(\theta_v) + \sin(\theta_{\rm LOS})\sin(\theta_v)\cos\phi_{\rm LOS}]. \quad (4)$$

The time-integrated spectrum can thus be calculated as[9] (see Equation (10) in Lundman et al. 2013)

$$F_E^{\rm ob}(\theta_v) = \frac{1}{4\pi d_L^2}\iint \frac{d\dot{N}_\gamma}{d\Omega} \times P_1(r, \Omega) \times P_2(r, \Omega, E) E d\Omega dr, \quad (5)$$

where $d\dot{N}_\gamma/d\Omega$ is the photon emission rate per unit solid angle from the base of the outflow ($r = r_0$).

In Equation (5), $d\dot{N}_\gamma/d\Omega = (L(\Omega)/4\pi)/2.7kT_0(\Omega)$, where $L(\Omega)$ is the isotropic luminosity per unit solid angle $d\Omega$ and $T_0(\Omega) = (L(\Omega)/4\pi r_0^2 ac)^{1/4}$ is the temperature at the base of the outflow per unit solid angle $d\Omega$. As a result, $d\dot{N}_\gamma/d\Omega$ is angle-dependent.

Since the typical luminosity may be low for a SGRB with a rapid decrease of luminosity in the lateral direction, the photosphere radius $R_{\rm ph}$ where the photons are being last-scattered may be smaller than the saturation radius for jet acceleration, $R_s = \eta(\theta) \cdot r_0$. We therefore must judge whether the acceleration is saturated ($R_{\rm ph} > R_s$) in each unit solid angle $d\Omega$ by calculating $R_{\rm ph}$ based on the assumption of saturation, and then deal with them for the calculations of P_1 and P_2 separately. Note that we have assumed a pure fireball here for simplicity. In principle, the outflow can be "hybrid," with an important contribution from a Poynting flux. The dynamics of such a scenario is more complicated, but the predicted photosphere spectrum would not be much different from the pure fireball case, even though the required parameters would be somewhat different. For a detailed treatment of a hybrid outflow, see Gao & Zhang (2015).

For the saturated case, $R_{\rm ph}$ is given by

$$R_{\rm ph} = \frac{1}{(1+\beta)\beta\eta^2(\theta)}\frac{\sigma_T}{m_p c}\frac{L(\theta)}{4\pi c^2\eta(\theta)}, \quad (6)$$

where σ_T is the Thompson cross-section, the Doppler factor is $D = [\eta(\theta) \cdot (1 - \beta(\theta) \cdot \cos\theta_{\rm LOS})]^{-1}$, the observer-frame temperature is $T^{\rm ob} = D(\Omega) \cdot T'(r, \Omega)$, and the comoving temperature $T'(r, \Omega)$ is

$$T'(r,\Omega) = \begin{cases} \dfrac{T_0(\Omega)}{2\eta(\Omega)}, & r < R_s(\Omega) < R_{\rm ph}(\Omega) \\ \dfrac{T_0(\Omega)\cdot[r/R_s(\Omega)]^{-2/3}}{2\eta(\Omega)}, & R_s(\Omega) < r < R_{\rm ph}(\Omega) \\ \dfrac{T_0(\Omega)\cdot[R_{\rm ph}(\Omega)/R_s(\Omega)]^{-2/3}}{2\eta(\Omega)}, & R_s(\Omega) < R_{\rm ph}(\Omega) < r \end{cases} \quad (7)$$

For the unsaturated case, $R_{\rm ph}$ is calculated by

$$R_{\rm ph} = \left[\frac{\sigma_T}{6m_p c}\frac{L(\theta)}{4\pi c^2\eta(\theta)}r_0^2\right]^{1/3}. \quad (8)$$

In this case, the Lorentz factor at the photosphere and the corresponding Doppler factor are given by $\Gamma(\theta) = R_{\rm ph}(\theta)/r_0$ and $D = [\Gamma(\theta) \cdot (1 - \beta(\theta) \cdot \cos\theta_{\rm LOS})]^{-1}$, respectively, and the comoving temperature is

$$T'(r, \Omega) = T_0(\Omega)/[2\Gamma(\Omega)]. \quad (9)$$

To calculate the time-resolved spectra, we add a δ-function $\delta(t - ru/\beta c)$ to Equation (5), where $u = (1 - \beta(\theta) \cdot \cos\theta_{\rm LOS})$. One then has

$$F_E^{\rm ob}(\theta_v, t) = \frac{1}{4\pi d_L^2}\iint \frac{d\dot{N}_\gamma}{d\Omega} \times P_1(r, \Omega) \times P_2(r, \Omega, E) \times \delta(t - \frac{ru}{\beta c}) E d\Omega dr. \quad (10)$$

With the above analysis, we can derive the time-resolved spectra for impulsive injection of energy and the time-integrated spectrum for continuous long-duration energy injection. For a realistic SGRB the duration for energy injection from the central engine is long (~1 s), as manifested by its observed duration(T_{90}).

2.3. Calculated Spectrum

The parameters of the jet structure and the viewing angle $\theta_{\rm v}$ adopted in our calculation are close to the best-fit values shown in Figure 1. We set the luminosity at the line of sight to be $\sim 10^{47}\,{\rm erg\,s^{-1}}$ to match the observation of GRB 170817A. According to SGRBs data, typically one has $L_0 \sim 10^{50}\,{\rm erg\,s^{-1}}$ and $\theta_{c,L} \simeq 6°$–$16°$ (Fong et al. 2015; Ghirlanda et al. 2016). For a power-law structured jet, the parameter q may be obtained through the luminosity dependence of the local event rate density $\rho_0(>L)$ of SGRBs (e.g., Zhang & Mészáros 2002a). Since $\rho_0(>L) \propto L^{-\lambda}$ ($\lambda \sim 0.7$) (Sun et al. 2015) and $\rho_0(>L) \propto \Omega(>E) \simeq \pi\theta^2$, the isotropic-equivalent luminosity $L \propto \theta^{-2/\lambda} \propto \theta^{-q}$, then $q \simeq 2.86$. Thus, we take $L_0 = 10^{50}\,{\rm erg\,s^{-1}}$, $\theta_{c,L} = 0.1$ rad, and $q = 3$ here. Meanwhile, we take the viewing angle $\theta_{\rm v}$ as 0.8 rad to match the luminosity mentioned above. With this viewing angle and other parameters we can obtain the approximate model spectrum and thus check whether we can perform a more detailed MCMC fit for the spectrum of GRB 170817A. Also, by comparing with the best-fit parameters (see Section 3) and the model spectrum for those best-fit parameters (shown in the bottom left panel of Figure 3), we can acquire the degree of change for the parameters corresponding to different model spectra. As for the bulk Lorentz factor, we let the value along the line of sight be in the range of (20–40) in order to match the peak energy (~100 keV) of the observed spectrum. In addition, we take $\eta \propto L^{1/4}$ according to the statistical results of a large sample of GRBs (Liang et al. 2010; Lü et al. 2012). Finally, we adopt $\eta_0 = 200$, $\theta_{c,\Gamma} = 0.1$ rad, and $p = q/4 = 0.75$.

The left panel of Figure 2 shows the calculated time-resolved spectra and the right panel is the time-integrated spectrum.[10]

[9] Note that Deng & Zhang (2014) provided a two-dimensional last-scattering probability function $P(r, \Omega)$. We adopt the separated probability function P_1 in this paper, since it is more easily generalized to structured jets and MCMC fitting.

[10] When calculating results in Figure 2 we do not make use of the best-fit parameters in Section 3 but rather use the example parameters, since the spectrum for the best-fit parameters is presented in the bottom left panel of Figure 3.

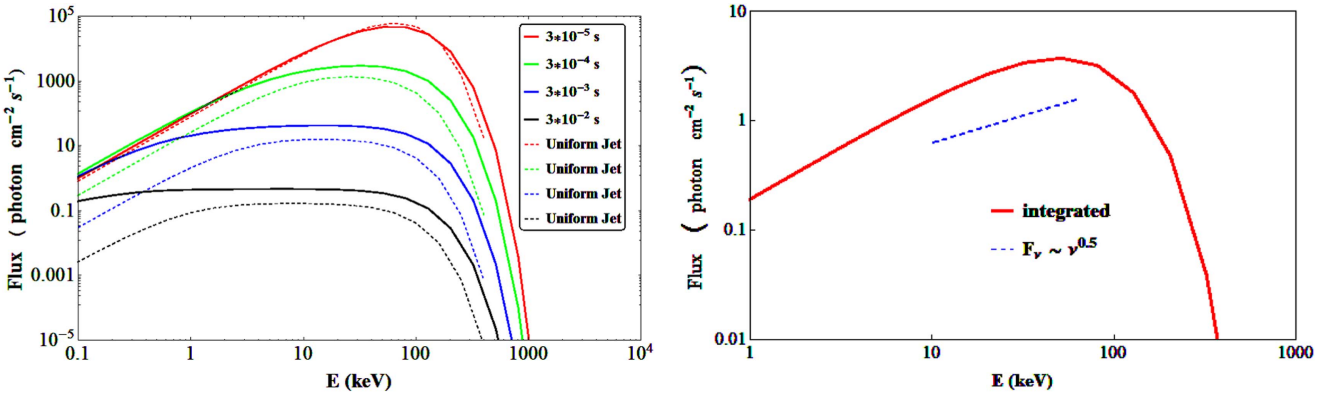

Figure 2. Calculated time-resolved spectra and the time-integrated spectrum. Left panel: the solid lines show the time-resolved spectra calculated with the parameters of the structured jet described in the text. The dashed lines show the time-resolved spectra calculated in Deng & Zhang (2014) for a uniform jet. For the case of a structured jet, the low-energy flux at later times is greatly boosted. Right panel: the time-integrated spectrum for the structured jet. The spectrum has a much softer low-energy photon index $\alpha \sim -0.5$ than blackbody and an exponential high-energy cutoff, which are close to the empirical fitting results of the main pulse spectrum of GRB 170817A.

Comparing the time-resolved spectra of a structured jet (solid lines in the left panel) and those of a uniform jet (dashed lines in the left panel), we can see that the low-energy power-law segment below the peak energy E_p is softer than the uniform jet case, and the total fluxes are also higher. This is because the low-energy emission has a significant contribution from the high latitudes with respect to the line of sight in the directions with smaller angles from the jet axis, where intrinsic luminosity is high but Doppler factor is low.

The low-energy photon index is $\alpha \sim -0.5$ for the time-integrated spectrum in the right panel. This is much softer than the case of the uniform jet ($\alpha \sim 0.5$, Deng & Zhang 2014). The origin of such a difference is again due to the enhanced near-axis high-latitude emission, likely caused by structures or changes in the Lorentz factor and luminosity. There are two effects here. First, the luminosity structure enhances the near-axis high-latitude emission. Second, the Lorentz factor structure also allows emission from some directions to become unsaturated, which would also contribute to the enhancement. The predicted low-energy photon index ($\alpha \sim -0.5$) of this model, as well as the exponential cutoff on the high-energy end, are consistent with the time-integrated spectrum of GRB 170817A, which can be empirically fitted by a cutoff power-law model with a low-energy photon index $\alpha \sim -0.6$ (Goldstein et al. 2017a; Zhang et al. 2018b). This encourages us to perform a more detailed MCMC fit of the data using our off-axis photospheric emission model from a structured jet.

3. Spectral Fitting of GRB 170817A with the Off-axis Photosphere Model

GRB 170817A was detected by *Fermi*-GBM and INTEGRAL SPI-ACS with a luminosity distance of $\simeq$40 Mpc (Abbott et al. 2017b). The analysis of the *Fermi*-GBM data showed two components: a main pulse from T0$-$0.26 s to T0 $+$0.57 s and a weak tail extending from T0$+$0.95 s to T0 $+$1.79 s (Goldstein et al. 2017a; Zhang et al. 2018b). In this work we choose the interval (i.e., between T0$-$0.3 s to T0 $+$0.4 s) with the most significant emission to perform the model fitting. We analyze the GBM Time Tagged Event (TTE) data from detectors NaI 1, NaI 2, and BGO 0. We fit the spectra using our photosphere model described in Section 2, using the McSpecFit package, which accepts a flexible user-defined spectral model (Zhang et al. 2016). A fit with the empirical cutoff power-law function was first performed. The spectrum of this interval is best fitted by the cutoff power-law model with a low-energy photon index of $-0.62^{+0.49}_{-0.54}$, peak energy $E_p = 145^{+140}_{-26}$ keV, and time-averaged flux of $(2.5^{+1.8}_{-1.0}) \times 10^{-7}$ erg cm^{-2} s^{-1}. The weak tail between T0$+$0.95 s and T0$+$1.79 s, with 34% the fluence of the main pulse, is best fitted by a blackbody spectrum with $kT = 11.3^{+3.8}_{-2.4}$ keV (Goldstein et al. 2017a; Zhang et al. 2018b).

A comparison between our photosphere model fitting and the cutoff power-law model fitting is shown in Figure 3. The best-fitting parameters are presented in Table 1 and also shown in Figure 1. It is apparent that our photosphere model can fit the data as well as the cutoff power-law model, with a PGSTAT/dof $= 260.9/357 = 0.73$ ($260.1/363 = 0.72$ for the cutoff power-law model). In addition, the residuals do not show any marked trends.

The parameter constraints of our photosphere model are illustrated in Figure 4. The best-fit values for the luminosity profile, $L_0 \sim 10^{49.16}$ erg s^{-1}, $\theta_{c,L} \sim 0.11$ rad, and $q \sim 2.99$, are consistent with the reasonable values of $L_0 = 10^{50}$ erg s^{-1}, $\theta_{c,L} = 0.1$ rad, and $q = 3$ (Fong et al. 2015; Sun et al. 2015; Ghirlanda et al. 2016). Also, the best-fit values for the bulk Lorentz factor profile, $\eta_0 \sim 388.82^{+82.2}_{-62.9}$ and $p \sim 0.42^{+0.52}_{-0.07}$ are close to the reasonable values of $\eta_0 = 200$ and $p = 0.75$. The best-fit viewing angle $\theta_v \sim 0.53^{+0.08}_{-0.17}$ rad falls into the reasonable range (0.65–0.72 rad in Granot et al. 2017a and 0.7 rad in Gottlieb et al. 2017). The observed luminosity[11] at the line of sight is $L \simeq 1.3 \times 10^{47}$ erg s^{-1}, which is consistent with the data (Goldstein et al. 2017a; Zhang et al. 2018b). The best-fit initial radius r_0 for acceleration is $\sim 10^{7.46}$ cm. We find that the acceleration is unsaturated ($R_{\rm ph} \sim 4.9 \times 10^8$ cm and $R_s \sim 5 \times 10^9$ cm) at the line of sight and the actual Lorentz factor[12] at the line of sight is $\Gamma \sim 17$.

The best-fit initial acceleration radius r_0 is $\sim 10^{7.46}$ cm. Bégué et al. (2017) gave an estimate of the r_0 based on the fitted peak energy and flux of a single blackbody in the observed spectrum (with the existence of a non-thermal

[11] Since the injected photons are almost emitted at the photosphere, the ratio of the observed temperature there to the temperature at the base T_0 represents the efficiency. In the saturated case, the efficiency is $(R_s/R_{\rm ph})^{2/3}$, while in the unsaturated case the efficiency is $\sim$1, which turns out to be the actual case.

[12] Note that Zou et al. (2018) got a Lorentz factor $\Gamma \sim 13.4$ for the case of an off-beaming relativistic jet.

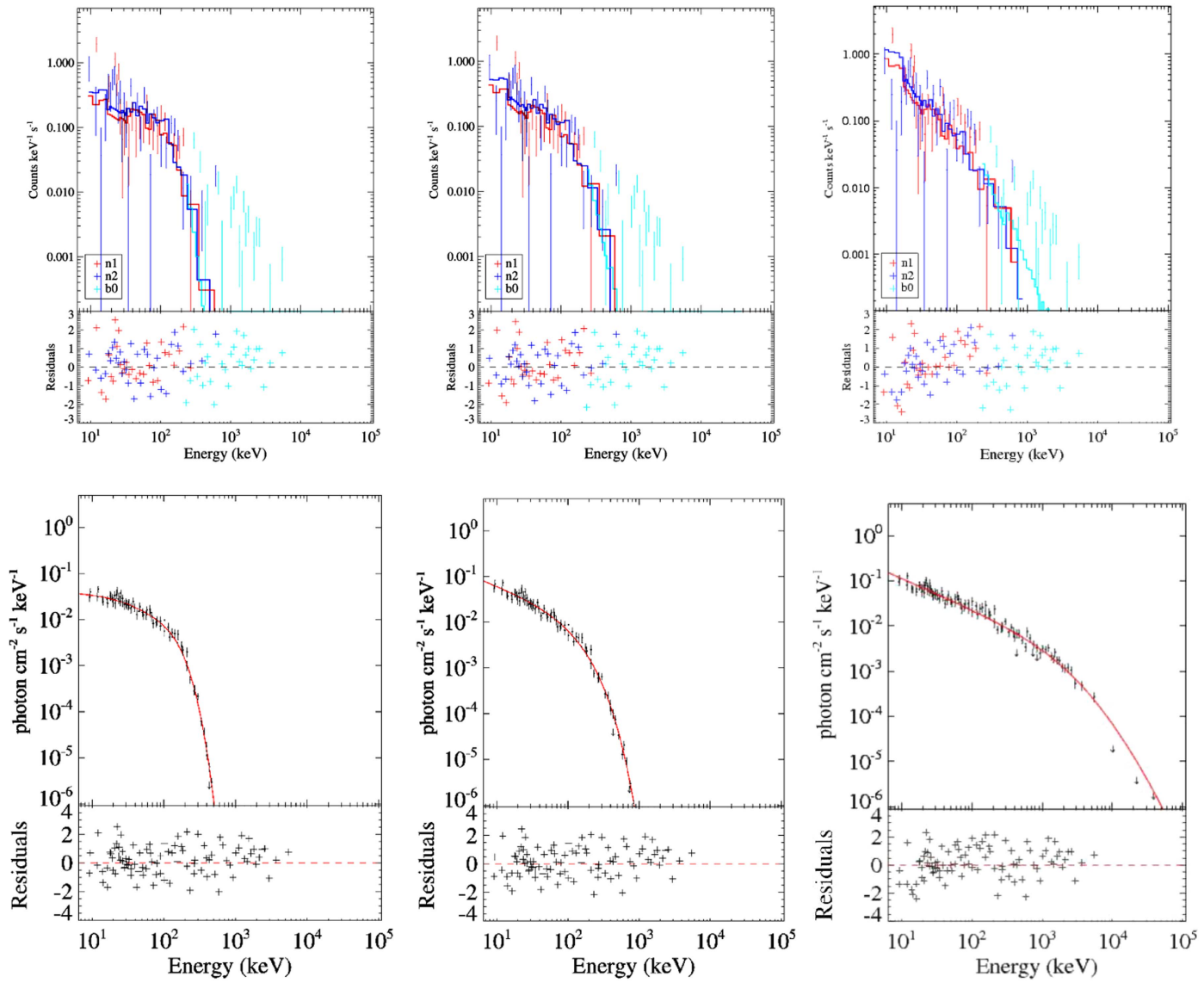

Figure 3. Comparisons among our photosphere model fitting, the cutoff power-law model fitting and the synchrotron model fitting for the time-integrated spectrum between −0.3 and 0.4 s. Top panels: observed count spectrum and model count spectrum for our photosphere model fitting (top left), the cutoff power-law model fitting (top middle) and the synchrotron model fitting (top right). Bottom panels: theoretical photon spectrum (red line) and observed photon flux (data points, which are obtained using the instrument responses to de-convolve the observed count spectrum) for our photosphere model fitting (bottom left), the cutoff power-law model fitting (bottom middle) and the synchrotron model fitting (bottom right). The legends of "n1, n2, b0" in the top panels indicate the two thallium-activated sodium iodide crystal detectors, referred to as NaI n1 and NaI n2, and one bismuth germanate crystal detector, referred to as BGO b0.

Table 1
Spectral Fitting Parameters Using the Off-axis Photosphere Model

Parameters	GRB 170817A
log L_0 (erg s^{-1})	$49.16^{+1.25}_{-0.18}$
$\theta_{c,L}$ (rad)	$0.11^{+0.01}_{-0.02}$
q	$2.99^{+0.46}_{-0.06}$
θ_v (rad)	$0.53^{+0.08}_{-0.17}$
η_0	$388.82^{+82.21}_{-62.90}$
p	$0.42^{+0.52}_{-0.07}$
log r_0 (cm)	$7.46^{+0.37}_{-0.30}$
log Norm	$0.28^{+0.58}_{-0.84}$

component) using the method of Pe'er et al. (2007), and found that r_0 is too small (3×10^6 cm, close to the innermost stable circular orbit of a black hole with $3\,M_\odot$) to justify the photosphere model. This seems to be in contradiction with our result. We would like to point out two significant differences between our photosphere model and theirs. First, the method to estimate the r_0 given in Pe'er et al. (2007) is only valid for the case of saturated acceleration ($R_{\rm ph} > R_s$). Thus, the unreasonable low r_0 only means that the photosphere model for saturated acceleration is unable to explain the data well. There is no conflict for our result (large r_0) because we are in the unsaturated regime. Second, their method relies on the assumption of a single blackbody contributed within a small cone along the line of sight, and an additional non-thermal component is needed to account for the observed spectrum. Our model, on the other hand, invokes a structured jet, so emission from high latitudes (relative to the LOS) is included in the calculation. The resulting spectrum is naturally a multi-color blackbody, which can account for the observed spectrum well

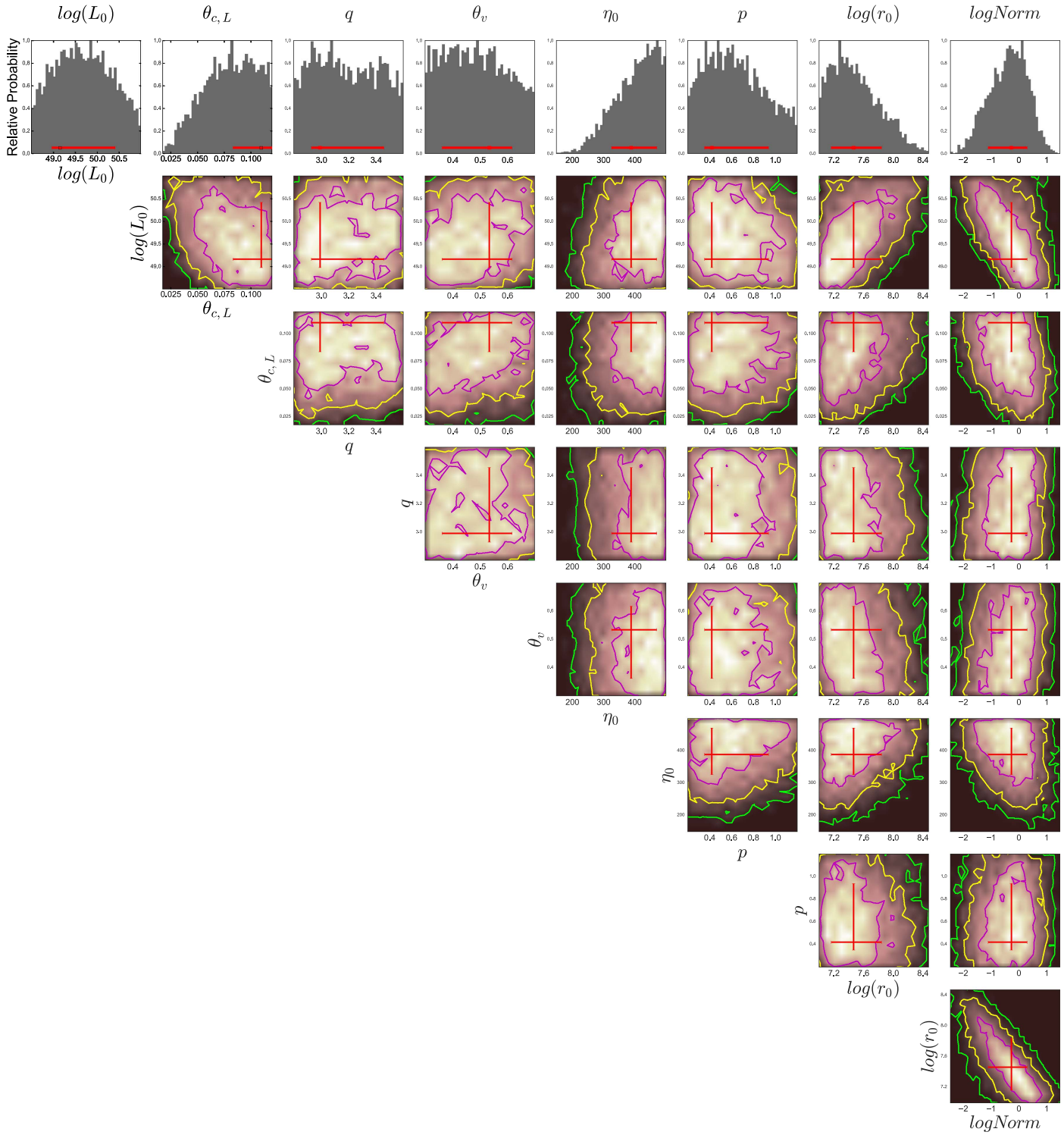

Figure 4. Parameter constraints of our photosphere model fitting for the time-integrated spectrum between −0.3 and 0.4 s. The histograms and contours illustrate the likelihood map. The red crosses show the best-fit values and 1σ error bars.

without the need of introducing a non-thermal component. As a result, our best-fit value r_0 is justified.

Furthermore, since the acceleration is in the unsaturated regime ($R_{\rm ph} < R_s$) along the line of sight, adiabatic cooling is not involved (unlike the saturated case, see Equation (7) and Equation (9)). As a result, the observed peak energy should be much higher than that in the saturated case for the same isotropic energy. This seems to be true for this burst (see Figure 3 in Zhang et al. 2018b).

4. Synchrotron Model Fitting

Synchrotron radiation from accelerated electrons in an optically thin region is another promising radiation mechanism for GRB prompt emissions. In this section, we apply a synchrotron radiation model to fit the spectra of GRB 170817A. To explain the hard low-energy spectrum, Uhm & Zhang (2014) proposed that fast-cooling electrons in a decaying magnetic field can form a hard electron distribution,

which results in a hard radiation spectrum (also see Derishev 2007). Since the observed spectral index is much harder than the standard fast-cooling spectrum ($\alpha = -1.5$) (Sari et al. 1998), we adopt the scenario of synchrotron radiation in a decaying magnetic field (Uhm & Zhang 2014) in our modeling.

Synchrotron radiation can in principle originate from internal shocks (Rees & Mészáros 1994) or a magnetic reconnection region (e.g., triggered by internal-collision-induced magnetic reconnection and turbulence, ICMART; Zhang & Yan 2011). The former is relevant for a matter-dominated fireball, which should be accompanied by a bright photosphere component. If one interprets the first pulse of GRB 170817A as being due to the synchrotron radiation, the lack of an earlier photosphere component suggests that the outflow is likely Poynting-flux-dominated, so the ICMART model may be more relevant.

Relativistic magnetic reconnection and the shock process are believed to be able to accelerate non-thermal particles and develop a power-law spectrum of the particle acceleration (see, e.g., Guo et al. 2014, 2016; Sironi & Spitkovsky 2014; Ardaneh et al. 2015). We assume that a group of electrons, which obey a power-law distribution, i.e., $Q(\gamma_{\rm e}', t') = Q_0(t')(\gamma_{\rm e}'/\gamma_{\rm m}')^{-p}$ for $\gamma_{\rm e}' > \gamma_{\rm m}'$, are injected in the relativistically moving shell of Lorentz factor Γ. Here, Q_0 is related to the injection rate $N_{\rm inj}'$ by $N_{\rm inj}' = \int_{\gamma_{\rm m}'}^{\gamma_{\rm max}'} Q(\gamma_{\rm e}', t') d\gamma_{\rm e}'$, where $\gamma_{\rm max}'$ is the maximum Lorentz factor of electrons. For an electron of $\gamma_{\rm e}'$, it would lose energy by synchrotron radiation, for which the cooling rate is

$$\dot{\gamma}_{\rm e}' = -\frac{\sigma_T B'^2 \gamma_{\rm e}'^2}{6\pi m_{\rm e} c}, \tag{11}$$

where B' is the magnetic field in the comoving frame. Recent studies reveal that synchrotron self-Compton (SSC) cooling may also play an important role in shaping the electron energy distribution (Bošnjak et al. 2009; Daigne et al. 2011; Geng et al. 2018). However, the effect of SSC cooling on the resulting spectra is similar to that of decaying magnetic fields. Here, for simplicity, we do not include it in our calculations and this does not markedly impact our main conclusions. Denoting the instantaneous spectrum of electrons as $\frac{dN_{\rm e}}{d\gamma_{\rm e}'}$, one can obtain it by solving the continuity equation in energy space (Longair 2011)

$$\frac{\partial}{\partial t'}\left(\frac{dN_{\rm e}}{d\gamma_{\rm e}'}\right) + \frac{\partial}{\partial \gamma_{\rm e}'}\left[\dot{\gamma}_{\rm e}'\left(\frac{dN_{\rm e}}{d\gamma_{\rm e}'}\right)\right] = Q(\gamma_{\rm e}', t'). \tag{12}$$

Considering a conical jet, the comoving magnetic field in the jet would decay with radius as

$$B' = B_0'\left(\frac{R}{R_0}\right)^{-1}, \tag{13}$$

where B_0' is the magnetic strength at R_0, and R_0 is the radius where the jet begins to emit the first photon we observed. In our modeling, we take $R_0 = 2\Gamma^2 c \times 1$ s, and denote observer-frame time since the first electron injection as $\hat{t}$ (in units of s) for an emission episode. We further introduce a parameter $t_{\rm off}$ to describe when the injection of electrons is turned off in the observer frame. Therefore, seven parameters in total are left free, i.e., Γ, $\gamma_{\rm m}'$, B_0', p, $N_{\rm inj}'$, $t_{\rm off}$, and $\hat{t}$. Unlike the calculation method for spectra adopted in Section 2, we only consider the emission from the region just near the LOS and treat this small region as a uniform jet. So relevant parameters in our calculation describe properties of the region near the LOS, rather than those of the jet axis. This treatment enables us to simplify the calculation and focus on properties of the region near the LOS. Unlike photosphere emission, for which one has considered the shape of the last-scattering surface that could be noticeably different for a structured jet, the synchrotron model is not affected by the jet structure if the Lorentz factor along the LOS is large enough (e.g., Zhang & Mészáros 2002a). This is valid for our case (our best-fit $\Gamma \sim 96$ along the LOS, so our simplification does not impact final results significantly).

We fit the spectra by interpolating our synchrotron model into the McSpecFit package (also see Zhang et al. 2018a, 2018b for details), and the fitting results are shown in Table 2 and Figure 5, with a PGSTAT/dof = 269.4/359. Compared with the PGSTAT/dof = 260.9/357 for the photosphere model, the PGSTAT/dof for the synchrotron model is slightly larger. However, this small difference could not help to prefer one model over the other.

One can perform a self-consistency check of the synchrotron model parameters. The GRB emission is delayed by $\Delta t \sim 1.7$ s with respect to the GW merger time (Abbott et al. 2017b; Zhang et al. 2018b). If one assumes that the jet is launched right after the merger, the distance the jet traveled at the time of magnetic dissipation is $R_{\rm GRB} \sim \Gamma^2 c\Delta t \sim 4.7 \times 10^{14}$ cm. Given the observed luminosity $L \sim 10^{47}$ erg s^{-1}, the comoving magnetic field in the emission region may be estimated as (e.g., Zhang & Mészáros 2002b) $B' \leqslant (2L/cR_{\rm GRB}^2)^{1/2}/\Gamma \sim 58$ G. The best-fit parameter falls within this range, suggesting the consistency of the model.

Our results suggest that the synchrotron model can also give a reasonable interpretation for the first pulse of the prompt emission of GRB 170817A. More complicated effects such as SSC (Geng et al. 2018) and slow heating/acceleration for electrons (Xu & Zhang 2017; Xu et al. 2018) have not been considered in our calculation. However, since these effects also tend to harden the spectrum, including them would also give a reasonable interpretation to the data, even though the best-fit parameters may be somewhat changed.

5. Discussion

5.1. The Blackbody in the Weak Tail

The spectrum of the weak tail emission of GRB 170817A is consistent with being a blackbody. Within our structured jet photosphere model, this may be interpreted as the transition from a structured jet to a roughly uniform jet at late times or the change of Lorentz factor and luminosity such that the contributions to observed flux from high latitudes are weakened. The softer peak energy is a natural result from the decrease of the luminosity and the Lorentz factor at late times. According to the best-fit results for the main pulse above, we have $L \sim 10^{47}$ erg s^{-1}, $\eta \sim 50$–150 at the line of sight. Thus, for the weak tail with $L \sim 0.3 \times 10^{47}$ erg s^{-1}, if the bulk Lorentz factor $\eta \sim 20$ (saturated acceleration with $R_{\rm ph} \sim 3.3 \times 10^9$ cm and $R_s \sim 5.8 \times 10^8$ cm), we may get a blackbody spectrum with $kT = 11.3^{+3.8}_{-2.4}$ keV. One should note that these are the average values within the entire duration of the weak tail.

Within the synchrotron model, the blackbody tail emission should be attributed to a different mechanism. One may

Table 2
Spectral Fitting Parameters Using the Synchrotron Model

Parameters	GRB 170817A
Γ	$95.57^{+4.43}_{-17.51}$
B_0' (G)	$5.45^{+8.96}_{-2.76}$
$\log \gamma_m'$	$5.82^{+0.001}_{-0.63}$
p	$2.85^{+0.05}_{-0.26}$
$\log R_{\rm inj}$ (s^{-1})	$44.98^{+0.02}_{-0.20}$
$t_{\rm off}$ (s)	$0.86^{+0.01}_{-0.54}$
$\hat{t}$ (s)	$0.70^{+0.05}_{-0.51}$

suppose that a successful structured jet breaks out to make the first pulse via synchrotron, and the more isotropic component breaks out the cocoon later to make the second thermal tail. Therefore, it is unable to rule out the synchrotron model based on the existence of the thermal tail.

5.2. The Time Delay between the GW Signal and the SGRB

The γ-ray emission onset of GRB 170817A has a delay of $\Delta t = 1.74 \pm 0.05$ s relative to the GW chirp signal (Abbott et al. 2017b). Under the framework of a photosphere model, some additional mechanism is required to account for such a delay. For instance, this delay may be attributed to the existence of a short-lived ($t_{\rm HMNS} \lesssim 1$ s) hypermassive NS (HMNS) after the NS–NS merger, and the jet is launched only after the hypermassive NS collapses into a black hole (e.g., Granot et al. 2017b). Such a type of NS–NS merger remnant is supported by previous numerical studies (e.g., Rosswog & Davies 2002; Rosswog et al. 2003). The delay onset of a relativistic jet relative to the merger is also required by the cocoon model (e.g., Gottlieb et al. 2017). After launching, the relativistic jet needs to break through the dynamical ejecta (e.g., Hotokezaka et al. 2013; Rosswog 2013) and/or neutrino driven wind, causing another time delay that could be a large fraction of a second (e.g., Moharana & Piran 2017; Nakar & Piran 2017).

Within the photosphere model, if one assumes $\Gamma \approx 2$–3 along the line of sight for the structured jet, the observed delay can be well explained without introducing an extra delay for the onset of the jet. In this case, however, the photosphere temperature is too low to explain the observed E_p. One needs to introduce some sub-photospheric dissipative processes to boost up E_p through Comptonization (Rees & Mészáros 2005; Giannios 2006; Bégué & Pe'er 2015; Vurm & Beloborodov 2016).

Within the synchrotron model, one does not need to invoke such a delayed jet launch with respect to the merger time. The delay can be accounted for by the timescale when the relativistic jet reaches the dissipation radius. It is intriguing that both the duration of the burst and the delay time are of the same order. Within the synchrotron model, both timescales are related to $R_{\rm GRB}/c\Gamma^2$, and therefore are comparable (Zhang et al. 2018b).

5.3. Comparison with the Cocoon Emission Model

Using the cocoon shock breakout to explain the γ-ray emission of GRB 170817A has been proposed lately (e.g., Gottlieb et al. 2017; Kasliwal et al. 2017; Bromberg et al. 2018). A delayed launch of the jet after the merger is needed to explain the data. In order to explain the soft low-energy photon index of the main pulse spectrum, both the cocoon shock breakout and our scenario attribute the soft emission below E_p to the superposition of a series of blackbody with different temperatures. The significant difference between their model and ours is the origin of low luminosity. In our model, the low luminosity is caused by the low luminosity of the structured jet along the line of sight, since we think that the jet may have a decreasing luminosity with angle and the viewing angle is large. The low luminosity of the cocoon shock breakout model arises from the low mass (thus low internal energy, $m_{\rm tail} \sim 4 \times 10^{-7} M_\odot$) of the fast ejecta tail, which emits γ-ray photons with a small Lorentz factor $\Gamma_s \approx 2$–3.

It is worth emphasizing that GRB 170817A appears to be a natural extension of short GRBs to the low-luminosity regime. The duration (T_{90}) and the peak energy of GRB 170817A are similar to a group of short GRBs (Lu et al. 2017; Zhang et al. 2018b). The average low-energy photon index ($\alpha \sim -0.69$, Burgess et al. 2017; Lu et al. 2017) for the complete short GRB sample of *Fermi*-GBM is close to the low-energy photon index ($\alpha \sim -0.62$) of this burst. The SGRB event rate density above a much lower luminosity threshold ($\sim 10^{47}$ erg s^{-1}), obtained by including GRB 170817A, is found to be consistent with the extension of the PL distribution for the normal SGRBs with higher luminosities (Zhang et al. 2018b). All these suggest that GRB 170817A may not have a very different origin from other short GRBs. The radiation mechanism for GRB 170817A is likely to be the same as that of other short GRBs with high luminosity. We believe that photosphere emission or synchrotron radiation from a structured jet with a large viewing angle is a natural explanation to the prompt emission data of GRB 170817A, and the cocoon model may not be needed to account for the data.[13] It has been suggested that the recent brightening of radio and X-ray fluxes is consistent with the prediction of the cocoon model (Kasliwal et al. 2017). On the other hand, the structured jet model can also explain the same data available so far (Lazzati et al. 2017b) as well as the late-time optical afterglow (Lyman et al. 2018).

6. Conclusions

As the first short GRB detected to be associated with an NS–NS merger event, GRB 170817A carries important clues for unveiling the underlying physics of SGRBs, including jet launching, interaction with the dynamical ejecta, energy dissipation mechanism, and radiation mechanism. The prompt emission data can be used to constrain these mechanisms.

In this paper, we focus on the spectral data of the first emission episode of GRB 170817A, and explore two models to account for the observed data. We find that both models can give reasonable fits to the data. In the first model, we developed a photosphere model in a structured jet. We found that the emission from the part closer to the jet axis can enhance the low-energy component of the spectrum, resulting in a softer low-energy photon index ($\alpha \sim -0.5$), which is consistent with the observation ($\alpha \sim -0.6$). We performed an MCMC fit of the spectrum from T0−0.3 s to T0+0.4 s using our model, and found that our model can give a comparable fit to the best-fit

[13] We stress that the cocoon may still exist in our models. But for our scenarios the outflow from the central engine can break out the cocoon quickly and naturally develop a structured jet, which is ahead of the slowly expanding cocoon. Further studies and detailed numerical simulations are needed to test this possibility, especially whether high Lorentz factors can be reached for the structured jet.

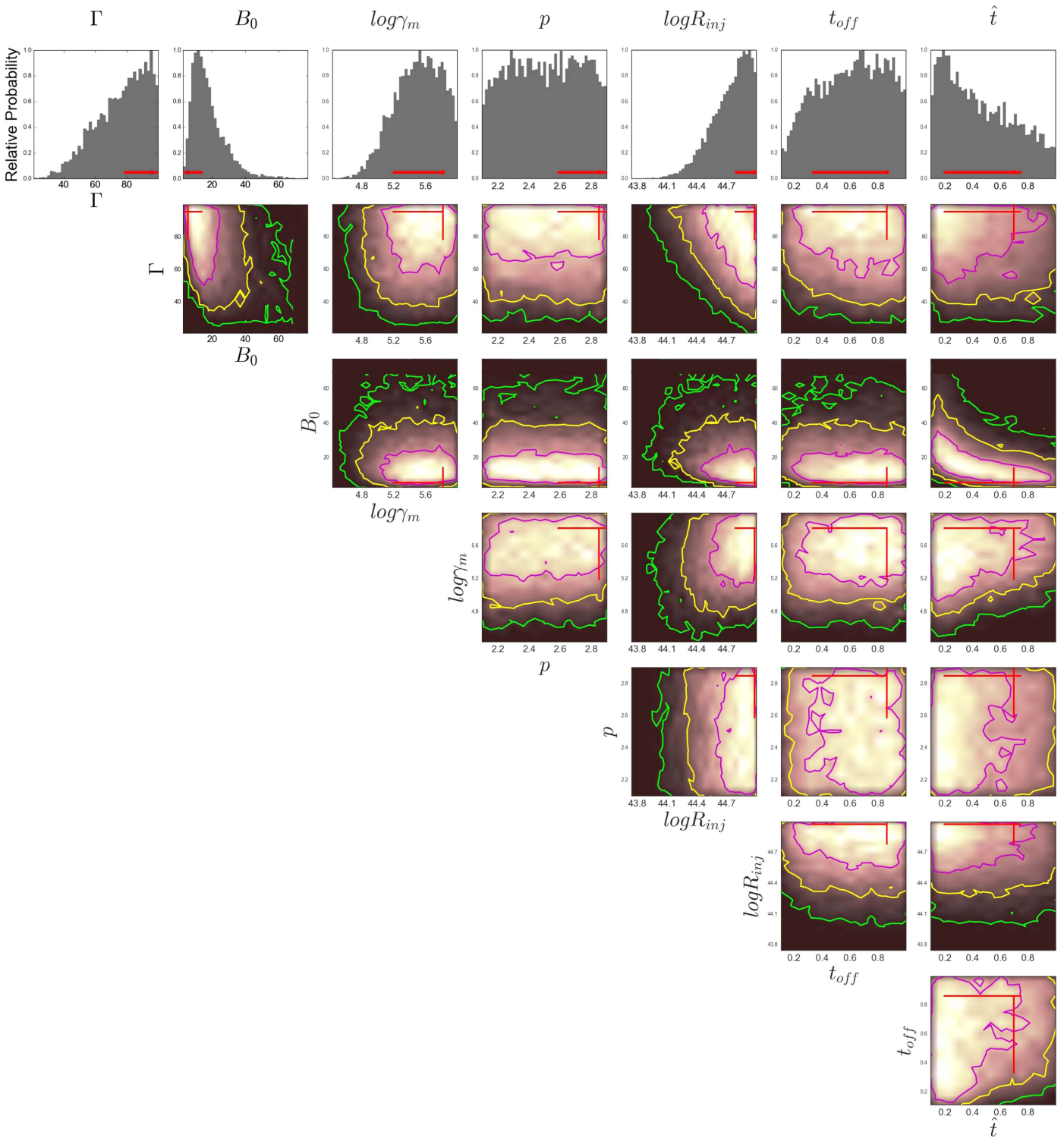

Figure 5. Parameter constraints of the synchrotron model fitting for the time-integrated spectrum between −0.3 and 0.4 s.

empirical model (the cutoff power-law model). The best-fit parameters are consistent with the results from some statistic works for SGRBs. In the second model, we consider synchrotron radiation in an optically thin region, with the jet expanding with a decaying magnetic field strength. This model also gives a reasonable fit to the data, even though a higher Lorentz factor along the line of sight is needed.

GRB 170817A is observed to be delayed from GW170817 by ∼1.7 s. Within the photosphere model, one needs to introduce a delay of the launch of the jet after the merger. Such a requirement is also needed by the cocoon shock break model. The synchrotron model does not demand such a delay time.

Bégué et al. (2017) discussed whether the typical emission models of synchrotron radiation and photospheric emission for structured and top-hat jets can explain the prompt emission of GRB 170817A, and found that these models are particularly challenging. They then proposed that the standard models for

SGRBs need to be modified. We reached an opposing conclusion by introducing a structured jet so that the observed spectrum is intrinsically a multi-color blackbody. Another difference is that jet acceleration is in the unsaturated regime. As we have shown, the photosphere model can give a very good fit to the data. For synchrotron radiation, we reached a set of best-fit parameters that are not unreasonable, in contrast to the conclusion of Bégué et al. (2017). We therefore conclude that both mechanisms are not ruled out by the data, and that the standard GRB mechanism (with a large viewing angle to a structured jet) can account for the prompt emission data of GRB 170817A without the need to invoke a different mechanism, e.g., cocoon shock breakout.

We thank the referee for the helpful suggestions. We acknowledge the use of the public data from the *Fermi* data archives. This work is supported by the National Basic Research Program ("973" Program) of China (grant No. 2014CB845800), the National Natural Science Foundation of China (grants No. 11725314, 11673068, 11433009, 11543005, 11603076, 11573014, 11533003, 11473012, 11722324, 11603003, 11633001, and 11690024), the Youth Innovation Promotion Association (2011231 and 2017366), the Key Research Program of Frontier Sciences (QYZDB-SSW-SYS005), the Strategic Priority Research Program "Multi-waveband gravitational-wave Universe" (grant No. XDB2300 0000) of the Chinese Academy of Sciences, and the Natural Science Foundation of Jiangsu Province (grant No. BK20161096). J.J.G. is supported by the National Postdoctoral Program for Innovative Talents (grant No. BX201700115) and China Postdoctoral Science Foundation funded project (grant No. 2017M620199). B.B.Z. acknowledges the support from the National Thousand Young Talents program of China.

ORCID iDs

Jun-Jie Wei https://orcid.org/0000-0003-0162-2488
Di Xiao https://orcid.org/0000-0002-4304-2759
He Gao https://orcid.org/0000-0002-3100-6558
En-Wei Liang https://orcid.org/0000-0002-7044-733X
Yong-Feng Huang https://orcid.org/0000-0001-7199-2906
Zi-Gao Dai https://orcid.org/0000-0002-7835-8585
Bing Zhang https://orcid.org/0000-0002-9725-2524

References

Abbott, B. P., Abbott, R., Abbott, T. D., et al. 2017a, PhRvL, 119, 161101
Abbott, B. P., Abbott, R., Abbott, T. D., et al. 2017b, ApJL, 848, L13
Abbott, B. P., Abbott, R., Abbott, T. D., et al. 2017c, ApJL, 848, L12
Abdo, A. A., Ackermann, M., Ajello, M., et al. 2009, ApJL, 706, L138
Abramowicz, M. A., Novikov, I. D., & Paczynski, B. 1991, ApJ, 369, 175
Aloy, M. A., Janka, H.-T., & Müller, E. 2005, A&A, 436, 273
Ardaneh, K., Cai, D., Nishikawa, K.-I., & Lembége, B. 2015, ApJ, 811, 57
Bégué, D., Burgess, J. M., & Greiner, J. 2017, ApJL, 851, L19
Bégué, D., & Pe'er, A. 2015, ApJ, 802, 134
Beloborodov, A. M. 2011, ApJ, 737, 68
Berger, E. 2014, ARA&A, 52, 43
Bromberg, O., Tchekhovskoy, A., Gottlieb, O., Nakar, E., & Piran, T. 2018, MNRAS, 475, 2971
Burgess, J. M., Greiner, J., Bégué, D., & Berlato, F. 2017, arXiv:1710.08362
Connaughton, V., Blackburn, L., Briggs, M. S., Broida, J., & Burns, E. 2017, LVC GRB Coordinates Network, 21506
Coulter, D. A., Foley, R. J., Kilpatrick, C. D., et al. 2017, Sci, 358, 1556
Dai, Z. G., & Gou, L. J. 2001, ApJ, 552, 72
Bošnjak, Ž, Daigne, F., & Dubus, G. 2009, A&A, 498, 677
Daigne, F., Bošnjak, Ž, & Dubus, G. 2011, A&A, 526, A110
Deng, W., & Zhang, B. 2014, ApJ, 785, 112
Derishev, E. V. 2007, Ap&SS, 309, 157
Eichler, D., Livio, M., Piran, T., & Schramm, D. N. 1989, Natur, 340, 126
Fong, W., Berger, E., Margutti, R., & Zauderer, B. A. 2015, ApJ, 815, 102
Gao, H., & Zhang, B. 2015, ApJ, 801, 103
Geng, J.-J., Huang, Y.-F., Wu, X.-F., Zhang, B., & Zong, H.-S. 2018, ApJS, 234, 3
Ghirlanda, G., Salafia, O. S., Pescalli, A., et al. 2016, A&A, 594, A84
Giannios, D. 2006, A&A, 457, 763
Goldstein, A., Veres, P., Burns, E., et al. 2017a, ApJL, 848, L14
Goldstein, A., Veres, P., von Kienlin, A., Blackburn, L., & Briggs, M. S. 2017b, LVC GRB Coordinates Network, 21528
Goodman, J. 1986, ApJL, 308, L47
Gottlieb, O., Nakar, E., Piran, T., & Hotokezaka, K. 2017, arXiv:1710.05896
Granot, J., Gill, R., Guetta, D., & De Colle, F. 2017a, arXiv:1710.06421
Granot, J., Guetta, D., & Gill, R. 2017b, ApJL, 850, L24
Guo, F., Li, H., Daughton, W., & Liu, Y.-H. 2014, PhRvL, 113, 155005
Guo, F., Li, X., Li, H., et al. 2016, ApJL, 818, L9
Hotokezaka, K., Kiuchi, K., Kyutoku, K., et al. 2013, PhRvD, 87, 024001
Jin, Z.-P., Li, X., Wang, H., et al. 2017, arXiv:1708.07008
Kasliwal, M. M., Nakar, E., Singer, L. P., et al. 2017, Sci, 358, 1559
Kathirgamaraju, A., Barniol Duran, R., & Giannios, D. 2018, MNRAS, 473, L121
Komissarov, S. S., Vlahakis, N., & Königl, A. 2010, MNRAS, 407, 17
Kumar, P., & Granot, J. 2003, ApJ, 591, 1075
Lamb, G. P., & Kobayashi, S. 2017, MNRAS, 472, 4953
Lazzati, D., Deich, A., Morsony, B. J., & Workman, J. C. 2017a, MNRAS, 471, 1652
Lazzati, D., Perna, R., Morsony, B. J., et al. 2017b, arXiv:1712.03237
Liang, E.-W., Yi, S.-X., Zhang, J., et al. 2010, ApJ, 725, 2209
Longair, M. S. 2011, High Energy Astrophysics (3rd ed.; Cambridge: Cambridge Univ. Press)
Lü, J., Zou, Y.-C., Lei, W.-H., et al. 2012, ApJ, 751, 49
Lu, R.-J., Du, S.-S., Cheng, J.-G., et al. 2017, arXiv:1710.06979
Lundman, C., Pe'er, A., & Ryde, F. 2013, MNRAS, 428, 2430
Lyman, J. D., Lamb, G. P., Levan, A. J., et al. 2018, arXiv:1801.02669
Mészáros, P. 2002, ARA&A, 40, 137
Mészáros, P., & Rees, M. J. 2000, ApJ, 530, 292
Mochkovitch, R., Hernanz, M., Isern, J., & Martin, X. 1993, Natur, 361, 236
Moharana, R., & Piran, T. 2017, MNRAS, 472, L55
Murguia-Berthier, A., Ramirez-Ruiz, E., Montes, G., et al. 2017, ApJL, 835, L34
Nakar, E. 2007, PhR, 442, 166
Nakar, E., & Piran, T. 2017, ApJ, 834, 28
Narayan, R., Paczynski, B., & Piran, T. 1992, ApJL, 395, L83
Paczynski, B. 1986, ApJL, 308, L43
Pe'er, A. 2008, ApJ, 682, 463
Pe'er, A., Barlow, H., O'Mahony, S., et al. 2015, ApJ, 813, 127
Pe'er, A., & Ryde, F. 2011, ApJ, 732, 49
Pe'er, A., Ryde, F., Wijers, R. A. M. J., Meszaros, P., & Rees, M. J. 2007, ApJL, 664, L1
Rees, M. J., & Mészáros, P. 1994, ApJL, 430, L93
Rees, M. J., & Mészáros, P. 2005, ApJ, 628, 847
Rossi, E., Lazzati, D., & Rees, M. J. 2002, MNRAS, 332, 945
Rosswog, S. 2013, RSPTA, 371, 20120272
Rosswog, S., & Davies, M. B. 2002, MNRAS, 334, 481
Rosswog, S., Ramirez-Ruiz, E., & Davies, M. B. 2003, MNRAS, 345, 1077
Rybicki, G. B., & Lightman, A. P. 1979, Radiative Processes in Astrophysics (New York: Wiley-Interscience)
Ryde, F. 2004, ApJ, 614, 827
Ryde, F. 2005, ApJL, 625, L95
Sapountzis, K., & Vlahakis, N. 2014, PhPl, 21, 072124
Sari, R., Piran, T., & Narayan, R. 1998, ApJL, 497, L17
Savchenko, V., Mereghetti, S., Ferrigno, C., Kuulkers, E., & Bazzano, A. 2017, LVC GRB Coordinates Network, 21507
Sironi, L., & Spitkovsky, A. 2014, ApJL, 783, L21
Sun, H., Zhang, B., & Li, Z. 2015, ApJ, 812, 33
Tchekhovskoy, A., McKinney, J. C., & Narayan, R. 2008, MNRAS, 388, 551
Thompson, C. 1994, MNRAS, 270, 480
Uhm, Z. L., & Zhang, B. 2014, NatPh, 10, 351
Vurm, I., & Beloborodov, A. M. 2016, ApJ, 831, 175
Xiao, D., Liu, L.-D., Dai, Z.-G., & Wu, X.-F. 2017, ApJL, 850, L41

Xu, S., Yang, Y.-P., & Zhang, B. 2018, ApJ, 853, 43
Xu, S., & Zhang, B. 2017, ApJL, 846, L28
Zhang, B., & Mészáros, P. 2002a, ApJ, 571, 876
Zhang, B., & Mészáros, P. 2002b, ApJ, 581, 1236
Zhang, B., & Yan, H. 2011, ApJ, 726, 90
Zhang, B.-B., Uhm, Z. L., Connaughton, V., Briggs, M. S., & Zhang, B. 2016, ApJ, 816, 72
Zhang, B.-B., Zhang, B., Castro-Tirado, A. J., et al. 2018a, NatAs, 2, 69
Zhang, B.-B., Zhang, B., Sun, H., et al. 2018b, NatCo, 9, 447
Zou, Y.-C., Wang, F.-F., Moharana, R., et al. 2018, ApJL, 852, L1